



Co-modification of Ni-based type Raney electrodeposits for hydrogen evolution reaction in alkaline media



I. Herraiz-Cardona, C. González-Buch, C. Valero-Vidal, E. Ortega, V. Pérez-Herranz*

Ingeniería Electroquímica y Corrosión (IEC), Departamento de Ingeniería Química y Nuclear, Universitat Politècnica de València, Camí de Vera s/n, 46022 Valencia, Spain

HIGHLIGHTS

- Ni and Ni–Co porous electrodes have been prepared by galvanic co-deposition.
- The incorporation of Co causes a surface morphology modification.
- HER on the investigated electrocatalysts proceeds via the Volmer–Heyrovsky mechanism.
- Co, in a range of 5–22 at.%, increases the intrinsic catalytic activity.

ARTICLE INFO

Article history:

Received 21 February 2013

Received in revised form

6 May 2013

Accepted 10 May 2013

Available online 18 May 2013

Keywords:

Raney type electrodes

NiCo alloys

Hydrogen evolution reaction

Surface roughness factor

ABSTRACT

In this work, high performance Ni and Ni–Co porous electrodes are prepared using the Raney strategy by galvanic co-deposition for hydrogen evolution reaction (HER) in alkaline solution (KOH 30 wt.%). The incorporation of Co into the Raney Ni matrix causes a surface morphology modification, from cracked to “cauliflower-like”, which dominates the superficial structure of the Co-richest obtained material. The evaluation of these electrodes as H₂-evolving cathodes is done through pseudo-steady-state polarization curves and electrochemical impedance spectroscopy (EIS). Ni Raney electrode (without Co) manifests the highest apparent catalytic activity per unit of geometric surface area, which is attributed to the higher surface roughness factor, determined by EIS. HER on the investigated electrocatalysts proceeds via the Volmer–Heyrovsky mechanism, with Heyrovsky as the rate-determining step (rds). From the kinetic parameters it is derived that Co presence, in a composition range of 5–22 at.%, increases the intrinsic catalytic activity of the developed cathodes per unit of true surface area, as a consequence of the synergism between the properties of Ni and of Co. Nevertheless, this improvement does not compensate the lower surface roughness factor, originated by the surface morphology modification as the Co content increases, reporting lower apparent catalytic activities.

© 2013 Elsevier B.V. All rights reserved.

1. Introduction

As an alternative to fossil fuels, hydrogen is considered one of the most promising energy carriers for the future because it is clean, has a high energy density and could be produced from renewable energy sources, manifesting complete environment friendliness [1]. Water electrolysis can generate high purity hydrogen and oxygen, and can be coupled with other renewable energy systems [2]. However, on current electrodes for water electrolysis, the high electrical power expenses restrain hydrogen large-scale application seriously [3]. In order to solve this problem,

many novel electrode materials were synthesized to reduce both the hydrogen evolution reaction (HER) overpotential (i.e. energy consumption) and the electrode cost [3,4]. Although platinum shows the highest activity for the hydrogen evolution reaction (HER), Ni-based materials have attracted more and more attention due to their good activity for HER and sufficient corrosion resistance in the alkaline solution at considerable lower cost [4–7].

The efficiency of the electrode materials can be improved by increasing the ratio between the real and geometric surface area of the electrode or by a synergistic combination of electrocatalytic components [4]. One of the common ways to enlarge the real surface area is the utilization of Raney-type alloys from which the active component (Al, Zn) is dissolved by an alkaline leaching, leading to pore and cavities formation. Various techniques have been developed for the preparation of this type of electrodes,

* Corresponding author. Tel.: +34 96 3877632; fax: +34 96 3877639.

E-mail address: vperez@iqn.upv.es (V. Pérez-Herranz).

consisting of powder pressing of Raney-Ni [7], electro co-deposition of Raney-Ni powder with Ni [8], electrodeposition of NiZn alloys [9–12] and thermal spraying of wires or powders [13,14]. On the other hand, the intrinsic activity of Ni has been enlarged by alloying with some metals or oxides such as: Ni–Co [9,10,12,15–17]; Ni–Mo [17–19]; Ni–W [19]; and Ni–CeO₂ [20]. With respect to Ni–Co alloys, Lupi et al. [15] found lower HER overpotentials in the case of Co concentrations ranging between 41 and 64 wt.%, attributing this intrinsic catalytic activity improvement to a synergism among the catalytic properties of nickel (low hydrogen overpotential) and of cobalt (high hydrogen adsorption) in this composition range. Domínguez-Crespo et al. [17] observed very high catalytic activity for HER on Ni₇₀Co₃₀ electrodes prepared by mechanical alloying, higher than that reported for Ni–Mo, Ni–Co–Mo, and Co–Mo alloys, attributing this behaviour to the increase in effective surface area of electrode by a diminishing in the grain size and synergetic combination.

In this work, different Ni–Co alloys were prepared by electrodeposition following the Raney porous material synthesis strategy, with the aim to combine the synergetic effect of the electrocatalytic materials alloy with very high electrode surface areas. The catalytic performance of the developed materials for HER was assessed in 30 wt.% KOH solution by means of pseudo-steady-state polarization curves and electrochemical impedance spectroscopy (EIS) techniques.

2. Experimental

2.1. Synthesis of electrodes

The metallic coatings were deposited onto AISI 304 stainless steel disc electrodes (0.5 cm² geometric area). Prior to use, these electrodes were set up with the pre-treatment process described in our previous works [9,10,16,21].

The electrodes were galvanostatically deposited at a current density of -50 mA cm^{-2} from a modified Watts bath (MWB) kept at 50 °C. Different CoSO₄ salt amounts were initially added to the MWB to obtain the Ni–Co alloys. Table 1 summarizes the bath compositions and the experimental conditions employed in the synthesis of electrodes. The reagents used for electrolyte preparation were of chemical grade and were not subjected to an additional purification. Distilled water was used to prepare electrolytes. The

Table 1
Operating conditions employed in the development of Ni and NiCo Raney electrodes.

Basic bath composition		g L ⁻¹
NiSO ₄ 6(H ₂ O)		330
NiCl ₂ 6(H ₂ O)		45
H ₃ BO ₃		37
ZnCl ₂		20
Co content in basic bath		
Electrode	g L ⁻¹ CoSO ₄ 7(H ₂ O)	Ni/Co ratio
NiR	—	—
NiCoR1	2.0	42.4
NiCoR2	23.9	3.6
NiCoR3	47.7	1.8
NiCoR4	71.6	1.2
NiCoR5	95.4	0.9
NiCoR6	190.8	0.4
Operating conditions		
Temperature/°C		50
j _d /mA cm ⁻²		50
Time min ⁻¹		60
pH		4.5

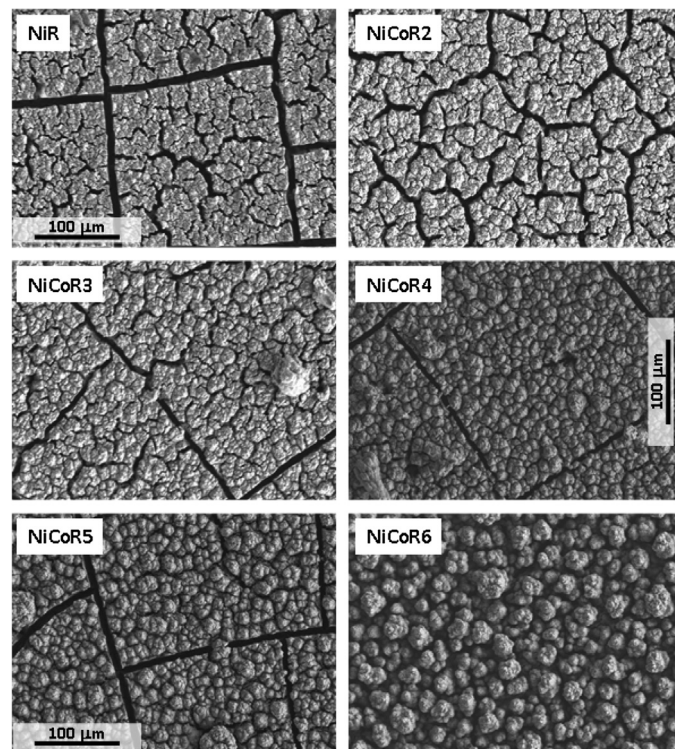


Fig. 1. SEM micrographs of the developed electrocatalytic layers.

as-deposited electrodes were treated in 6 M NaOH at 50 °C during 48 h in order to selectively dissolve a part of the electrodeposited zinc, generating a porous coating with a very high surface area [7–14].

Electrodepositions were carried out in a thermostated one-compartment cell. The electrolyte inside the cell (50 mL) was agitated by means of a magnetically driven stirrer so as to avoid the generated gas bubbles remaining on the substrate surface. The counter electrode was a high purity large-area graphite electrode. The reference electrode was commercially available silver–silver chloride (Ag–AgCl) electrode with 3 M potassium chloride (KCl) solution. The experiments were accomplished by using an AUTOLAB PGSTAT302N potentiostat/galvanostat.

The structures, morphologies and compositions of the developed electrocatalytic coatings were examined by means of a JEOL JSM-3600 scanning electron microscope coupled with an Energy-Dispersive X-Ray (EDX).

2.2. Electrochemical measurements

HER on the synthesized electrocatalysts was accomplished by pseudo-steady-state polarization curves and electrochemical impedance spectroscopy (EIS). All these tests were performed in oxygen free 30 wt.% KOH solutions, which were achieved by bubbling N₂ before the experiments.

Polarization curves were potentiodynamically recorded from $-1.60 \text{ V vs Ag/AgCl}$ (-1.40 V vs SHE) up to the equilibrium potential, at a scan rate of 1 mV s^{-1} , and at six different temperatures: 30, 40, 50, 60, 70 and 80 °C. Before the tests, the working electrode was held at $-1.60 \text{ V vs Ag/AgCl}$ (-1.40 V vs SHE) in the same solution for the time needed to establish reproducible polarization curves.

EIS measurements were performed after obtaining the polarization curves. AC impedance measurements were carried out at different cathodic overpotentials, and at 30, 50, and 80 °C. The

measurements were made in the frequency range of 10 kHz–3 mHz. Ten frequencies per decade were scanned using a sinusoidal signal of 10 mV peak-to-peak. The complex nonlinear least square (CNLS) fitting of the impedance data was carried out with the Zview 3.0 software package.

The electrochemical measurements were carried out in the electrochemical cell P200002526. In this system, the developed electrode was used as the working electrode and it was positioned in such a way that the electrode/electrolyte interface was on a vertical plane, so as to allow, when necessary, the free release of the hydrogen bubbles produced. A large-area Ni foam (INCOFOAM™) was employed as counter electrode, and the reference electrode was the same as that used in the electrodeposition process. All the electrochemical experiments were performed using an AUTOLAB PGSTAT302N potentiostat/galvanostat.

3. Results and discussion

Fig. 1 shows the SEM micrographs of the developed electrocatalysts used as cathodes for HER studies after the activation (zinc leaching) treatment. It is seen that the morphology of the electrodes synthesized from less Co concentrated baths (Ni/Co bath ratio >1) consists of cracks and micro-cracks distributed along the surface. As the bath Co content increases it is observed an electrode structure/morphology transformation, from cracked to nodular “cauliflower-like” structure, being the latter the morphology that completely dominates the surface of the NiCoR6 electrode.

Table 2 shows the chemical composition analysis of the developed electrodes obtained by means of EDX. As it was expected, the deposit Co content directly increases with the bath Co content. Attempts to obtain Co contents higher than 21.5 at.% (adding higher Co salt amounts to the electrodeposition bath) lead to weak and easily removable layers. This phenomenon may be attributed to the very high bath concentration, which increases the electrolyte viscosity affecting the correct ionic species distribution along the substrate surface. After the alkaline leaching, there is still a high Zn percentage in the coatings. Nevertheless, according to the preferential deposition of Zn in these systems [22], the remaining Zn must be occluded within a Ni or Ni–Co layer.

The cathodic polarization curves of the HER obtained for different selected electrocatalysts at 50 °C in 30 wt.% KOH solution are displayed in **Fig. 2a**. In order to clarify the result presentation, it has been only taken into account the results obtained on NiR, NiCoR2, NiCoR4, and NiCoR6 electrodes, since an intermediate behaviour has been observed for the other electrodeposits. A single value for the Tafel slope is observed for all the materials between –0.05 and –0.18 V, indicating that the HER on these electrodes is a purely kinetically controlled reaction described by the Tafel equation [23]. Polarization curves were fitted by a linear regression, which provided the values of the Tafel slope, b , the exchange current densities, j_0 , and the charge transfer coefficient, α , summarized in **Table 3**. According to the literature of HER on

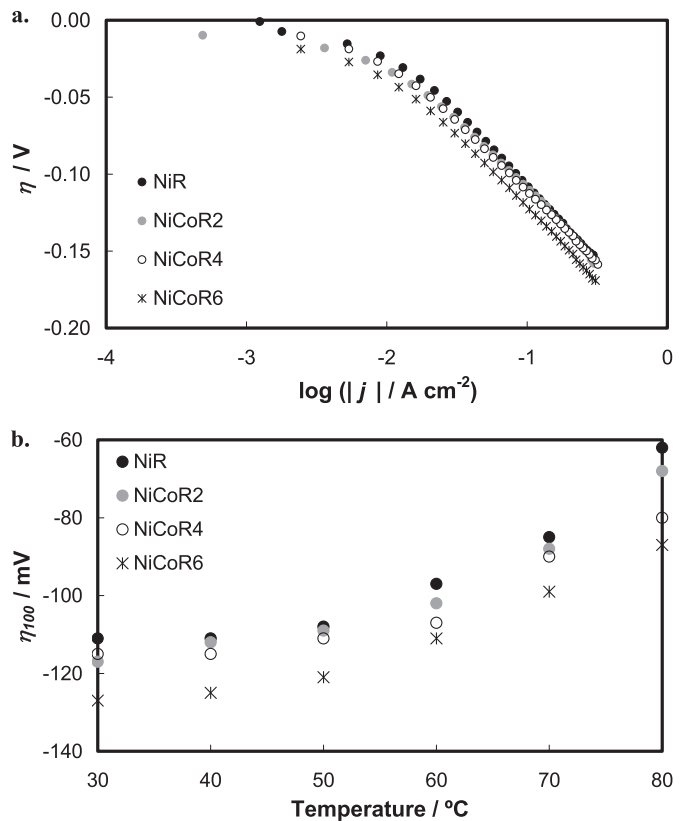
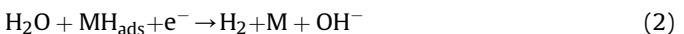
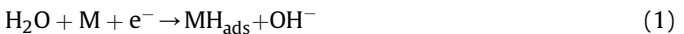


Fig. 2. a. Linear Tafel polarization curves at 50 °C and b. overpotentials at a current density of -100 mA cm^{-2} , η_{100} , recorded on the investigated electrocatalytic coatings in 30 wt.% KOH solution.

transition metals and the kinetic parameters shown in **Table 3**, b ranging from 75 to 120 mV dec⁻¹ at 30 and 80 °C, respectively, and α close to 0.5 for all the coatings, HER proceeds via the same Volmer (1)–Heyrovsky (2) mechanism [4,5,19]:



Nevertheless, it is necessary to know about the surface coverage

Table 3

HER kinetic parameters obtained from the polarization curves recorded on the developed electrocatalytic layers in 30 wt.% KOH solution at different temperatures.

Electrode	Temperature / °C					
	30	40	50	60	70	80
NiR	83.8	85.0	97.3	101.9	124.2	131.3
$b/\text{mV dec}^{-1}$	0.72	0.73	0.66	0.65	0.55	0.53
$j_0/\text{mA cm}^{-2}$	2.9	3.5	6.9	11.2	20.6	24.3
NiCo2	75.1	76.8	95.1	92	112.1	112.1
$b/\text{mV dec}^{-1}$	0.80	0.81	0.67	0.72	0.61	0.62
$j_0/\text{mA cm}^{-2}$	2.9	3.5	6.9	11.2	20.6	24.3
NiCo4	72.1	75.9	90.8	99.4	99.4	112.7
$b/\text{mV dec}^{-1}$	0.83	0.82	0.71	0.66	0.68	0.62
$j_0/\text{mA cm}^{-2}$	2.5	3.1	6.0	9.68	12.4	20.2
NiCo6	76.7	87.6	92.5	95.2	95.8	101.1
$b/\text{mV dec}^{-1}$	0.78	0.71	0.69	0.69	0.71	0.69
$j_0/\text{mA cm}^{-2}$	2.3	4.0	4.9	6.8	9.2	13.8

Table 2
Superficial composition of the developed electrocatalytic layers determined by EDX.

Electrode	Ni/Co bath ratio	at.%			Ni/Co deposit ratio
		Ni	Co	Zn	
NiR	–	59.6	–	40.4	–
NiCoR1	42.4	56.1	1.9	42.0	29.5
NiCoR2	3.6	56.5	2.7	40.8	20.9
NiCoR3	1.8	54.4	3.3	42.3	16.5
NiCoR4	1.2	55.8	6.0	38.2	9.3
NiCoR5	0.9	54.5	10.5	35.0	5.2
NiCoR6	0.4	50.7	21.5	27.8	2.4

by adsorbed hydrogen, θ , in order to establish the rate determining step (rds) when the Tafel slope is ca. 120 mV dec $^{-1}$ due to the fact that if $\theta \rightarrow 0$, Volmer is rds ; and if $\theta \rightarrow 1$, Heyrovsky is rds [5,23].

Not considerable differences in the electrocatalytic behaviour of the developed electrodes were observed from the polarization curves of Fig. 2a. Thus, the overpotential values at a fixed current density of -100 mA cm $^{-2}$, η_{100} , were reported and plotted as a function of temperature in Fig. 2b in order to facilitate the comparative study. The η_{100} values obtained for the investigated electrocatalysts reveal an electrochemical activity higher and/or in the same magnitude order than those previously reported by other authors for Raney-Ni, NiMo, NiLa, Ni/MoS₂, NiP, etc. [4]. The catalytic activity of the electrodes increases with temperature, which is the expected kinetic behaviour. According to Fig. 2b, the highest apparent catalytic activity is reported for the NiR electrode, decreasing with the Co content and, hence, with the progressive growth of the globular or “cauliflower-like” morphology. The same conclusion can be derived from the study of the exchange current densities, j_0 , reported in Table 2, increasing j_0 with the temperature. Fig. 3a demonstrates that this increase is linear in a semi-logarithmic plot, which is in accordance with the Arrhenius law [24]:

$$\log j_0 = A_0 - \frac{E_a}{2.303 \cdot R} \cdot \frac{1}{T} \quad (3)$$

where E_a (J mol $^{-1}$) represents the apparent activation energy for the HER, and A_0 (A cm $^{-2}$) is the pre-exponential factor. The catalytic activity of an electrode in a given electrolyte is usually evaluated by means of the E_a value. The lower the E_a , the lower the energy requirements for hydrogen production. Fig. 3b shows the E_a calculated from the slopes of the regression lines plotted in Fig. 3a, as a function of the electrode Co content. The obtained E_a values are very close to that postulated in literature for similar electrode materials when HER takes place via the Volmer–Heyrovsky mechanism, being the electrochemical desorption the rds [24–26]. Activation energy values decreases from an atomic Co percentage of ca. 5%, where a maximum is reached. This fact indicates a higher intrinsic catalytic activity of Co-richest electrodes (NiCoR4 and NiCoR6), which may be attributed to the synergism between the properties of Ni and of Co, previously reported by other authors [15,17], in the composition range of these alloys.

The “a priori” disagreement between the results derived from j_0 and η_{100} values (apparent activity) and from E_a values (intrinsic activity) may be solved by knowing the real electrochemically

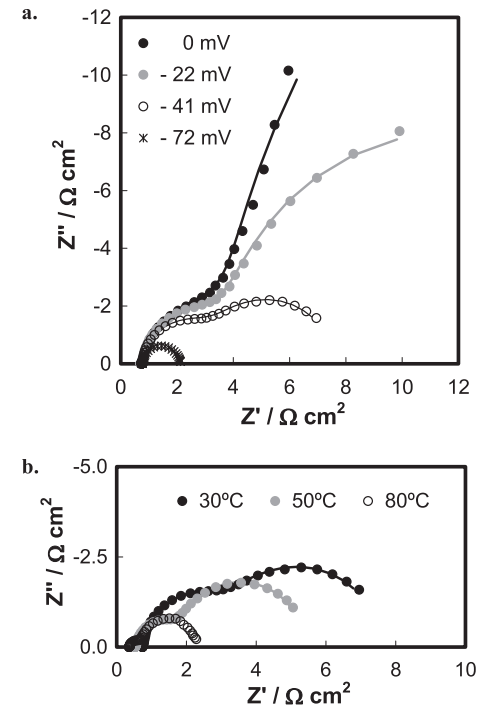


Fig. 4. Nyquist representation of the impedance data obtained for the NiCoR6 electrocatalyst in 30 wt.% KOH solution at: a. 30 °C (effect of overpotential); and b. -38 ± 4 mV (effect of temperature). Symbols are the experimental points and solid lines are modelled data.

active surface area, which can be estimated by electrochemical impedance spectroscopy (EIS) [14]. This technique also permits us to extract information on the kinetics of the HER. EIS response obtained on all the developed electrocatalysts is characterized by two deformed semicircles (i.e. two times constants) in the complex plane plot, the first one at high frequencies (HF), and the second one at low frequencies (LF). Fig. 4 shows the effect of both the cathodic overpotential (Fig. 4a) and the temperature (Fig. 4b) on the Nyquist plots of the impedance of the NiCoR6 electrocatalyst. From Fig. 4 it is clear that the diameter of both semicircles considerably decreases with both the cathodic overpotential and temperature, indicating that both semicircles are related to the electrode kinetics [13]. The same behaviour was also reported for the other electrodes. As it was discussed in previous papers [9,10],

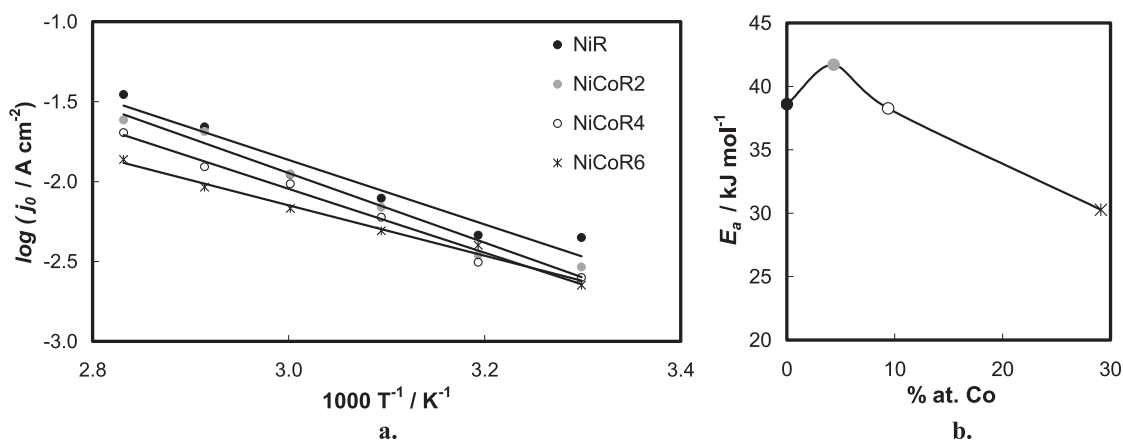


Fig. 3. a. Electrochemical Arrhenius plot of the exchange current density at the reversible potential for HER on the investigated electrocatalytic layers in 30 wt.% KOH solution. b. Effect of Co content on the apparent activation energy, E_a , for the investigated electrocatalytic layers.

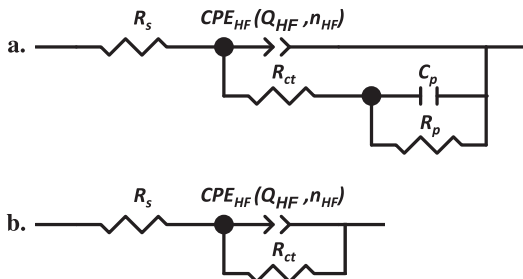


Fig. 5. EEC models used to explain the EIS response of the HER on the investigated electrodes: a. two-time constant parallel model (2 TP); b. one-time constant model (1 T).

the two-time constants parallel (2 TP) electric equivalent circuit (EEC), initially proposed by Armstrong and Henderson [27] and presented in Fig. 5a, properly models and describe the AC response of Raney Ni and Ni–Co electrodeposits. The 2 TP model reflects the response of a HER system characterized by two-time constants, the HF time constant, τ_{HF} , related to the charge-transfer kinetics, and the LF time constant, τ_{LF} , associated to the hydrogen adsorption [13,16,28]. Fig. 4a manifests that at the more negative overpotential (-72 mV) the semicircle related to the adsorption relaxation apparently completely disappears and only the semicircle related to the charge transfer remains observable. This is due to the fact that the adsorption process is facilitated and

Table 4

EEC parameters obtained by fitting EIS experimental spectra recorded at various overpotentials and temperatures in 30 wt.% KOH solution on the NiCoR6 electrocatalyst.

Parameter	30 °C			
η/V	0	-0.022	-0.041	-0.072
χ^2	$3.86 \cdot 10^{-4}$	$2.23 \cdot 10^{-4}$	$1.56 \cdot 10^{-4}$	$1.18 \cdot 10^{-3}$
$R_s/\Omega \text{ cm}^2$	0.77	0.75	0.76	0.77
$R_{ct}/\Omega \text{ cm}^2$	4.95	4.34	3.25	1.35
$Q_{HF}/\Omega^{-1} \text{ cm}^{-2} \text{ s}^\phi$	0.555	0.378	0.288	0.206
n_{HF}	0.91	0.93	0.95	0.95
$C_{dl}/\text{F cm}^{-2}$	0.506	0.340	0.264	0.183
$R_p/\Omega \text{ cm}^2$	40.6	14.6	3.4	—
$C_p/\text{F cm}^{-2}$	2.31	2.36	2.77	—
τ_{HF}/s	0.39	0.26	0.20	0.14
τ_{LF}/s	93.8	34.4	9.5	—
Parameter	50 °C			
η/V	0	-0.020	-0.040	-0.072
χ^2	$2.55 \cdot 10^{-4}$	$1.60 \cdot 10^{-4}$	$1.43 \cdot 10^{-4}$	$1.65 \cdot 10^{-3}$
$R_s/\Omega \text{ cm}^2$	0.53	0.53	0.55	0.54
$R_{ct}/\Omega \text{ cm}^2$	6.35	2.86	1.61	0.94
$Q_{HF}/\Omega^{-1} \text{ cm}^{-2} \text{ s}^\phi$	0.371	0.321	0.260	0.202
n_{HF}	0.95	0.95	0.95	0.89
$C_{dl}/\text{F cm}^{-2}$	0.339	0.292	0.230	0.146
$R_p/\Omega \text{ cm}^2$	55.1	16.3	3.2	—
$C_p/\text{F cm}^{-2}$	2.11	2.14	2.27	—
τ_{HF}/s	0.18	0.15	0.13	0.08
τ_{LF}/s	116.3	35.0	7.3	—
Parameter	80 °C			
η/V	0	-0.017	-0.033	-0.062
χ^2	$8.83 \cdot 10^{-4}$	$2.69 \cdot 10^{-4}$	$4.39 \cdot 10^{-4}$	$6.56 \cdot 10^{-4}$
$R_s/\Omega \text{ cm}^2$	0.36	0.36	0.37	0.37
$R_{ct}/\Omega \text{ cm}^2$	1.64	0.77	0.41	0.36
$Q_{HF}/\Omega^{-1} \text{ cm}^{-2} \text{ s}^\phi$	0.341	0.313	0.233	0.227
n_{HF}	0.93	0.90	0.93	0.84
$C_{dl}/\text{F cm}^{-2}$	0.289	0.235	0.185	0.126
$C_p/\text{F cm}^{-2}$	1.62	1.63	1.85	19.31
$R_p/\Omega \text{ cm}^2$	30.6	7.1	1.5	0.05
τ_{HF}/s	0.10	0.08	0.07	0.05
τ_{LF}/s	49.6	11.6	2.8	0.97

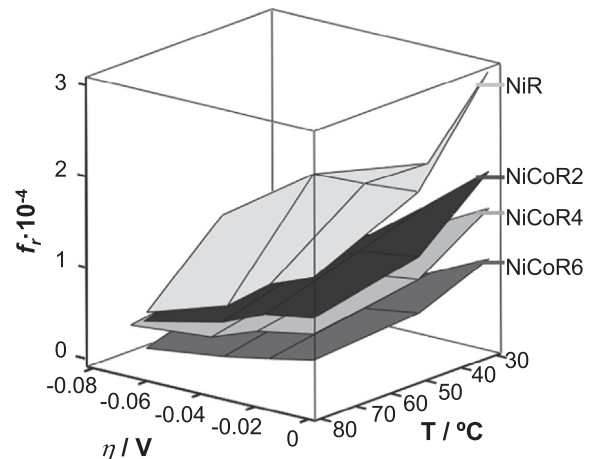


Fig. 6. 3D representation of the roughness factor, f_r , obtained for the investigated electrocatalytic layers in 30 wt.% KOH solution.

the charge-transfer process dominates the impedance response as the cathodic potential increases. Hence, HER is controlled by Heyrovsky step [29–31]. In such a case, the one-time constant model (1 T), see Fig. 5b, is used to describe the impedance response. For both EEC, the double layer capacitance (C_{dl}) was replaced by a constant phase angle element (CPE) [5,13]. CPE is defined in impedance representation as:

$$Z_{\text{CPE}} = [Q \cdot (i\omega)^n]^{-1} \quad (4)$$

where Q is the CPE constant, ω is the angular frequency (in rad s⁻¹), $i^2 = -1$ is the imaginary number, and n is the CPE exponent.

Table 4 shows the best-fit estimates of the different 2 TP/1 T EEC parameters obtained from the impedance measurements recorded on the NiCoR6 at different temperatures and overpotentials. The average double layer capacitances related to the charge-transfer kinetics, C_{dl} , for the catalytic coatings were determined using the relation suggested by Brug et al. [32]:

$$C_{dl} = \left[Q_{HF} \left/ \left(R_S^{-1} + R_{ct}^{-1} \right)^{(1-\alpha_{HF})} \right. \right]^{1/\alpha_{HF}} \quad (5)$$

where Q_{HF} and α_{HF} are the components of the CPE_{HF} ; and R_s and R_{ct} are the solution and the charge transfer resistances, respectively. As it can be concluded from Table 4, the trend of EEC parameters with respect to the overpotential is in agreement with the phenomenon which represent: on the one hand, both C_{dl} and R_{ct} decrease with the cathodic potential, indicating an improvement of HER; on the other hand, the hydrogen adsorption pseudocapacitance, C_p , increases whereas the associated resistance, R_p , diminishes with an increase in the cathodic potential, which is the typical behaviour related to the response of hydrogen adsorbed on the electrode surface [13,19,31,33].

The real active surface area, in terms of surface roughness factor (f_r), may be estimated by comparing the C_{dl} related to the HER charge-transfer kinetics of porous/rough and smooth electrodes [34]. C_{dl} value depends on the metal composition by means of the equation (6) [35]:

$$C_{dl} = \sum_i \theta_{Mi} \cdot C_{dlMi} \quad (6)$$

where θ_{Mi} is the surface percentage occupied by metal M_i , whose double layer capacitance is C_{dlMi} . In this case, due to the fact that the atomic radii of Ni and Co have similar values, the surface

Table 5

Exchange current densities, j_0 , corrected with the surface roughness factor, f_r , obtained for the investigated electrocatalytic layers in 30 wt.% KOH solution.

Electrode	Corrected exchange current density ($j_0 \cdot f_r^{-1}$)/ $\mu\text{A cm}^{-2}$)		
	30 °C	50 °C	80 °C
NiR	0.16	0.40	2.43
NiCoR2	0.15	0.55	2.42
NiCoR4	0.17	0.60	2.46
NiCoR6	0.24	0.77	2.54

percentage occupied by each metal can be approximated to the atomic percentage obtained by EDX. According to literature and our experimental confirmation, they were selected values of $20 \mu\text{F cm}^{-2}$ [6,11] and $135 \mu\text{F cm}^{-2}$ [36] for the double layer capacitance of smooth polycrystalline pure Ni and Co electrodes, respectively. Fig. 6 presents the 3D diagram of the surface roughness factors, f_r , determined for the investigated cathodes at the different operating conditions. Both the increase in temperature and overpotential lead to a decrease in the f_r , due to the surface blockage effect of the increase in the hydrogen bubbles generation. The highest f_r obtained values correspond to the NiR electrode, diminishing this parameter with the increase in the Co content. Accordingly with the SEM study (see Fig. 1), this effect is attributed to the surface morphology transition, from cracked to globular/“cauliflower-like”, as the Co content increases. Exchange current densities corrected with the obtained surface roughness factor, $j_0 \cdot f_r^{-1}$, for all the investigated catalysts are reported in Table 5. As it is clear, the corrected exchange current densities increase with the presence of Co, from a Co content higher than 5 at.% (NiCoR2 electrode). This indicates that the presence of Co, in the composition range of NiCoR4 and NiCoR6 electrodes, increases the intrinsic catalytic activity for HER. Nevertheless, this improvement does not compensate the decrease in the roughness factor associated to the surface morphologic change, and lower apparent catalytic activities are reported for these materials.

From the study of both polarization curves and EIS, it can be estimated that HER on the developed electrodes is carried out by the Volmer–Heyrovsky mechanism, with the electrochemical desorption as rds. Accordingly, the current density of the reaction can be written as:

$$j = j_{\text{H}} = 2Fk_{\text{H}}\theta e^{\frac{-\beta_H F\eta}{RT}} \quad (7)$$

and θ can be determined assuming the pseudo-equilibrium hypothesis of the Volmer reaction and the Langmuir electrochemical adsorption isotherm:

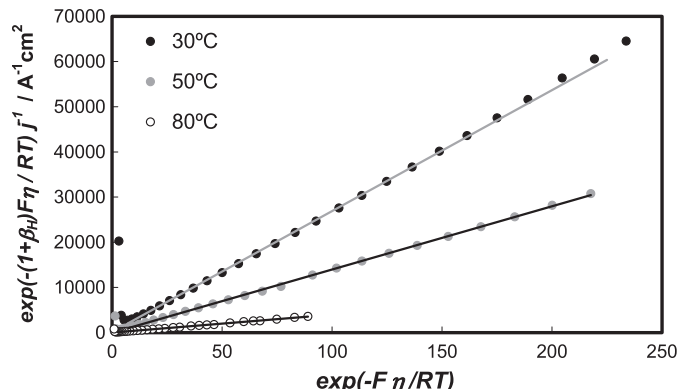


Fig. 7. Testing of the Heyrovsky-controlling mechanism for HER on the NiCoR2 electrocatalyst at different temperatures.

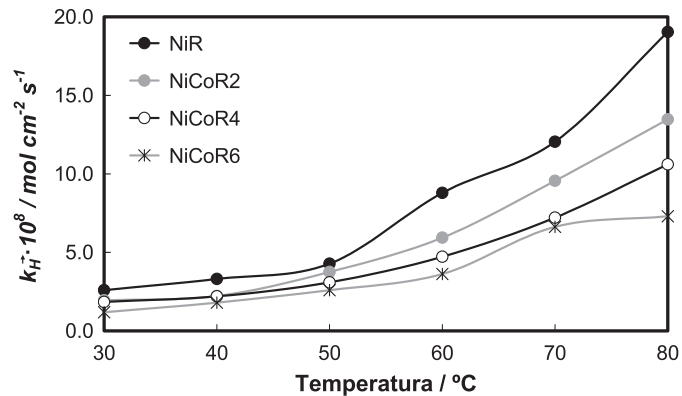


Fig. 8. Comparison of the rate constants, k_{H} , on the investigated electrocatalytic layers for the Volmer–Heyrovsky HER mechanism (electrochemical desorption considered as rds), as a function of temperature.

$$\theta = \frac{K_V e^{\frac{-F\eta}{RT}}}{1 + K_V e^{\frac{-F\eta}{RT}}} \quad (8)$$

where $F (=96,485 \text{ C mol}^{-1})$ is the Faraday constant; $R (=8.314 \text{ J mol}^{-1} \text{ K}^{-1})$ is the gas constant; β_H is the Heyrovsky symmetry factor equals the charge-transfer coefficient, α , [23]; k_{H} is the Heyrovsky rate constant; and K_V represents the quotient between the direct, k_{V} , and reverse, k_{V}^{-1} , Volmer rate constants.

Note that rate constants include concentrations of OH^- and H_2O .

Substituting the expression for the coverage (8) into the expression for the current (7), one obtains

$$j = j_{\text{H}} = 2Fk_{\text{H}} \frac{K_V e^{\frac{-F\eta}{RT}}}{1 + K_V e^{\frac{-F\eta}{RT}}} e^{\frac{-\beta_H F\eta}{RT}} \quad (9)$$

which can be rearranged to give:

$$\frac{e^{\frac{-(1+\beta_H)F\eta}{RT}}}{j} = \frac{1}{2Fk_{\text{H}}} e^{\frac{-F\eta}{RT}} + \frac{1}{2Fk_{\text{H}} K_V} \quad (10)$$

Therefore, a plot of $\exp[-(1+\beta_H)F\eta/RT]/j$ against $\exp[-F\eta/RT]$ should give a straight line of slope $1/2Fk_{\text{H}}$ and intercept $1/2Fk_{\text{H}} K_V$ [37,38]. As shown in Fig. 7 for the NiCoR2 electrode, good linearity is obtained over almost the whole range of η . The linear regression has been restricted to high cathodic overpotentials, taking into account that the model expression is based on the high-field approximation. The same behaviour was reported for all the developed electrodes indicating applicability of the electrochemical-desorption-controlled mechanism. From the slope and the intercept of this kind of plots, both k_{H} and K_V have been easily evaluated for each electrode at the different operating temperatures. Fig. 8 compares the Heyrovsky direct rate constants, k_{H} , obtained for the chosen electrodes as a function of temperature. The obtained values are in the same magnitude order than that reported by other authors on porous Ni based electrodes in alkaline media, where HER is electrochemical-desorption controlled [8,12,31]. As it is clear from Fig. 8, k_{H} values increase exponentially with temperature, following the Arrhenius law. In fact, from the slope of the semi-logarithmic plot of the rate constants it can be obtained activation energy values very close to that determined from the exchange current densities, corroborating the selected HER mechanism. The increase in k_{H} values with temperature is

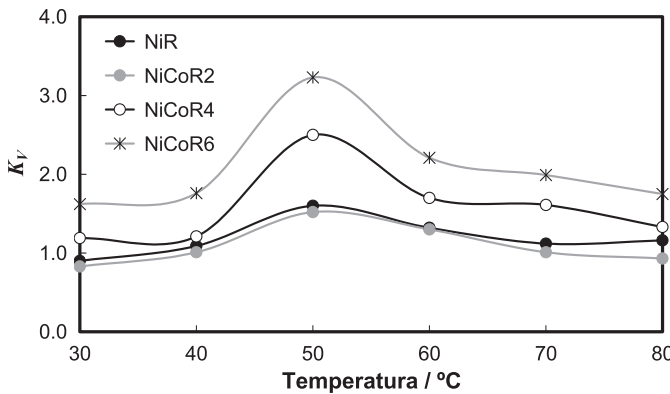


Fig. 9. Comparison of the pseudo-equilibrium constants, K_V , on the investigated electrocatalytic layers for the Volmer–Heyrovsky HER mechanism (electrochemical desorption considered as rds), as a function of temperature.

attributed to the improvement of the intrinsic catalytic property of these materials. The highest k_{H}^{-} values, i.e. the highest apparent catalytic activity, are obtained for the NiR electrode, whereas these kinetic constants decrease with the electrode Co content, as it was also concluded from j_0 and η_{100} values (note that the parameter k_{H}^{-} is also influenced by the electrode surface area). On the other hand, the effect of temperature on the pseudo-equilibrium constant K_V , obtained for the investigated electrodes, is displayed in Fig. 9. This parameter manifests a maximum value at 50 °C in all the cases, indicating that higher temperatures do not favour the hydrogen adsorption on the electrode surface [12]. Fig. 9 shows that K_V values increase with the Co content, from Co concentrations higher than 5 at.%. K_V parameter is not influenced by the roughness factor (because it is defined as the quotient of the Volmer rate constants) so the above mentioned result indicates that the presence of Co, at certain composition range, favours the electrochemical desorption step due to the synergism between the properties of Ni and Co, shifting the Volmer pseudo-equilibrium to the formation of the adsorbed specie (MH_{ads}) and, therefore, improving the electrode intrinsic catalytic activity. This effect confirms the lower E_a and the higher $j_0 \cdot f_r^{-1}$ values obtained as the Co electrode charge increases.

4. Conclusions

On the basis of the presented results it can be concluded that type Raney Ni and Ni–Co electrodes manifest a very high activity at relatively high overpotentials which is important for commercial application. Co-modification of type Raney Ni-based electrodes does not improve the apparent catalytic activity of these materials as cathodes for HER in alkaline media, the NiR electrode (without Co) being the best overall electrocatalyst. The incorporation of Co into the electrodeposition bath results in an electrode surface morphology change, from a cracked to a nodular/“cauliflower-like” morphology, characterized by a lower surface roughness factor (determined by EIS). HER on the developed electrodes takes place via the Volmer–Heyrovsky mechanism, being the electrochemical desorption the rds. As it was evidenced from E_a and K_V values, the presence of Co, at a composition range higher than 5 at.%, increases the intrinsic catalytic activity of cathodes, as a consequence of the synergistic combination. Nevertheless, the increase in the intrinsic activity does not compensate the lower cathode surface area and,

therefore, Co-richest materials reported the highest $|\eta_{100}|$ and the lowest j_0 and k_{H}^{-} values.

Acknowledgements

Isaac Herraiz-Cardona is grateful to Fundación Iberdrola for the economical support by means of the Project: “Desarrollo y caracterización de materiales electródicos porosos estables para la producción de hidrógeno a partir de la electrólisis alcalina del agua” – II Convocatoria de Ayudas a la Investigación en Energía y Medio Ambiente. The authors would like to thank the financial support from Generalitat Valenciana (PROMETEO/2010/023) and Universidad Politécnica de Valencia (PAID-06-10-2227).

References

- [1] S.S. Penner, Energy 31 (2006) 33–43.
- [2] A.G. Garciaconde, F. Rosa, Int. J. Hydrogen Energy 18 (1993) 995–1000.
- [3] K. Zeng, D. Zhang, Prog. Energy Comb. Sci. 36 (2010) 307–326.
- [4] A. Lásia, in: W. Vielstich, H.A. Gasteiger, A. Lamm (Eds.), *Handbook of Fuel Cells—Fundamentals, Technology and Applications, Electrocatalysis*, vol. 2, John Wiley & Sons, Ltd., 2003, pp. 416–440.
- [5] A. Lásia, A. Rami, J. Electroanal. Chem. 294 (1990) 123–141.
- [6] A. Rami, A. Lásia, J. Appl. Electrochem. 22 (1992) 376–382.
- [7] LL. Chen, A. Lásia, J. Electrochem. Soc. 139 (1992) 3214–3219.
- [8] Y. Choquette, L. Brossard, A. Lásia, H. Menard, Electrochim. Acta 35 (1991) 1251–1256.
- [9] I. Herraiz-Cardona, E. Ortega, V. Pérez-Herranz, Electrochim. Acta 56 (2011) 1308–1315.
- [10] I. Herraiz-Cardona, E. Ortega, L. Vázquez-Gómez, V. Pérez-Herranz, Int. J. Hydrogen Energy 36 (2011) 11578–11587.
- [11] LL. Chen, A. Lásia, J. Electrochem. Soc. 138 (1991) 3321–3328.
- [12] M.J. Giz, G. Tremiliosi-Filho, E.R. González, Electrochim. Acta 39 (1994) 1775–1779.
- [13] L. Birry, A. Lásia, J. Appl. Electrochem. 34 (2004) 735–749.
- [14] A. Kellenberger, N. Vaszilcsin, W. Brandl, J. Solid State Electrochem. 11 (2007) 84–89.
- [15] C. Lupi, A. Dell'Era, M. Pasquali, Int. J. Hydrogen Energy 34 (2009) 2101–2106.
- [16] I. Herraiz-Cardona, E. Ortega, J. García Antón, V. Pérez-Herranz, Int. J. Hydrogen Energy 36 (2011) 9428–9438.
- [17] M.A. Domínguez-Crespo, M. Plata-Torres, A.M. Torres-Huerta, E.M. Arce-Estrada, J.M. Hallen-López, Mater. Charact. 55 (2005) 83–91.
- [18] A. Damian, S. Omanovic, J. Power Sources 158 (2006) 467–476.
- [19] E. Navarro-Flores, Z. Chong, S. Omanovic, J. Mol. Catal. A: Chem. 226 (2005) 179–197.
- [20] Z. Zheng, N. Li, C.-Q. Wang, D.-Y. Li, F.-Y. Meng, Y.-M. Zhu, J. Power Sources 222 (2013) 88–91.
- [21] I. Herraiz-Cardona, E. Ortega, L. Vázquez-Gómez, V. Pérez-Herranz, Int. J. Hydrogen Energy 37 (2012) 2147–2156.
- [22] A. Brenner, *Electrodeposition of Alloys: Principles and Practice*, vol. 2, Academic Press Inc., New York, 1963.
- [23] Southampton Electrochemistry Group, *Instrumental Methods in Electrochemistry*, Wiley, New York, 1985.
- [24] O. Savadogo, E. Ndzebet, Int. J. Hydrogen Energy 26 (2001) 213–218.
- [25] J.O.M. Bokris, A.K.N. Reddy, *Modern Aspects of Electrochemistry*, vol. 2, Plenum Press, New York, 1970.
- [26] A.N. Correia, S.A.S. Machado, Electrochim. Acta 43 (1998) 367–373.
- [27] R.D. Armstrong, M. Henderson, J. Electroanal. Chem. 39 (1972) 81–90.
- [28] D.A. Harrington, B.E. Conway, Electrochim. Acta 32 (1987) 1703–1712.
- [29] L. Bai, D.A. Harrington, B.E. Conway, Electrochim. Acta 32 (1987) 1713–1731.
- [30] A. Lásia, in: B.E. Conway, R.E. White (Eds.), *Modern Aspects of Electrochemistry*, vol. 35, Kluwer Academic/Plenum Publishers, New York, 2002, pp. 1–49.
- [31] N.A. Assunção, M.J. Giz, G. Tremiliosi-Filho, E.R. Gonzalez, J. Electrochem. Soc. 144 (1997) 2794–2800.
- [32] G.J. Brug, A.L.G. Vandeneeden, M. Sluytersrehbach, J.H. Sluyters, J. Electroanal. Chem. 176 (1984) 275–295.
- [33] R. Simpraga, G. Tremiliosi-Filho, S.Y. Qian, B.E. Conway, J. Electroanal. Chem. 424 (1997) 141–151.
- [34] S. Trasatti, O.A. Petri, Pure Appl. Chem. 63 (1991) 711–734.
- [35] L. Vázquez-Gómez, S. Cattarin, P. Guerreiro, M. Musiani, J. Electroanal. Chem. 634 (2009) 42–48.
- [36] A. Jukic, J. Piljac, M. Meticoš-Hukovic, J. Mol. Catal. A: Chem. 166 (2001) 293–302.
- [37] B.E. Conway, D.M. Novak, J. Chem. Soc. Faraday Trans. 1 (75) (1979) 2454–2472.
- [38] S. Ferro, A. De Battisti, J. Phys. Chem. B 106 (2002) 2249–2254.